Supporting Information: Landau-Ginzburg theory of cortical dynamics: scale-free avalanches emerge at the edge of synchronization

Serena di Santo[a,b,c,1], **Pablo Villegas**[a,1], **Raffaella Burioni**[b,c], **and Miguel A. Muñoz**[a,2]

[a]Departamento de Electromagnetismo y Física de la Materia e Instituto Carlos I de Física Teórica y Computacional. Universidad de Granada. E-18071, Granada, Spain; [b]Dipartimento di Fisica e Scienza della Terra, Università di Parma, via G.P. Usberti, 7/A - 43124, Parma, Italy; [c]INFN, Gruppo Collegato di Parma, via G.P. Usberti, 7/A - 43124, Parma, Italy

SI1. Robustness of the results against changes in the dynamics. In this appendix we confirm the robustness of the results and conclusions presented in the main part with respect to the modification of diverse ingredients and modeling details. In particular, we *first* discuss the full model including synaptic plasticity (as in the main text), but without truncating the equation for activity in a series expansion and, *second*, we consider inhibition as encapsulated in the well-known Wilson-Cowan equations (rather than synaptic plasticity) as a chief regulatory mechanism.

Non-truncated excitatory-activity equation. The dynamics in a single mesoscopic region of the cortex or "unit" is described by the full Wilson-Cowan equation (1) for the excitatory activity –such that the activity grows with the incoming current through a sigmoid response function– together with the Tsodyks-Markram TM model for synaptic plasticity (2):

$$\begin{cases} \dot{\rho} = & -a\rho + (1-\rho)\tanh\left(\rho R - \Theta\right) + h \\ \dot{R} = & \frac{1}{\tau_R}\left(\xi - R\right) - \frac{1}{\tau_D}\rho R. \end{cases} \quad [1]$$

In Figure 1, we illustrate that a linear-stability analysis reproduces a Hopf bifurcation scenario, as in the most relevant case (case A) discussed in the paper. When noise and spatial coupling are added, and the system is studied on a two-dimensional lattice, a synchronous irregular regime of network spikes, as well as an asynchronous irregular regime of nested oscillations –fully analogous to their corresponding counterparts in the the main text– are found, as graphically illustrated by the lower panels of Figure 1. This unveils the existence of a synchronization transition and confirms that the simplified truncated equation for the activity considered in the main text is a valid approximation of the full dynamics. Here we do not show a detailed analysis of the synchronization transition nor of the emergence of scale-free avalanches; but, let us remark that we have not found any substancial qualitative difference with respect to the case discussed in the paper in any of our exploratory checks.

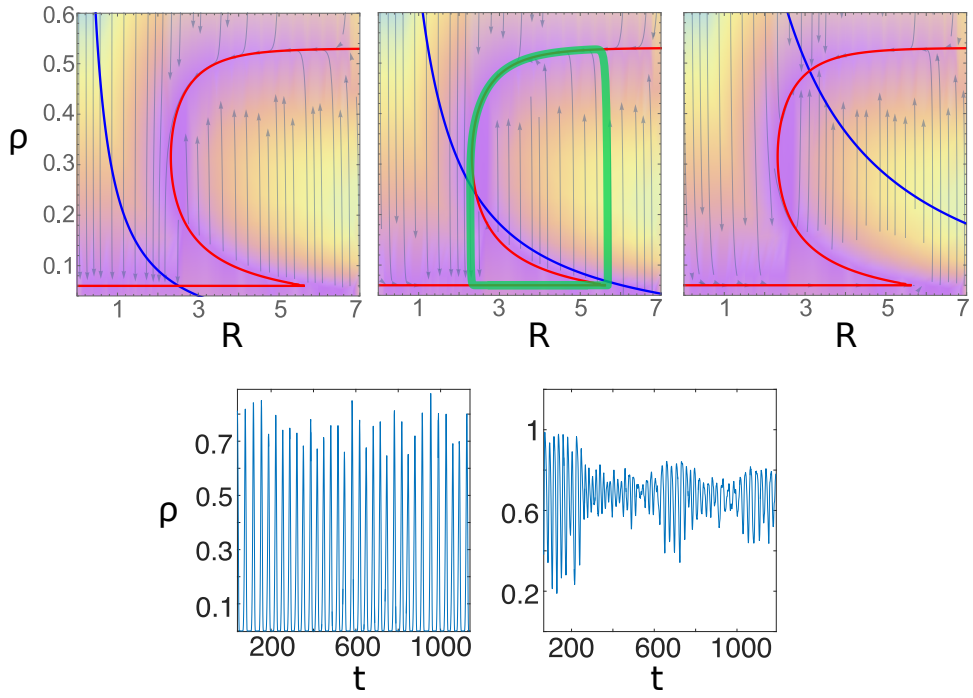

Fig. 1. Analysis of the model of Eq. 1. Upper panels: deterministic phase portrait with $\xi = 5, 12, 28$ (from left to right). respectively. showing a down state, a limit cycle and up state regimes, as in the case A of the main text. Other parameters are $a = 1$, $\tau_D^{-1} = 0.033$, $\tau_R = 500$, $\Theta = 0.34$, $h = 0.06$. Varying parameter values, it is possible to find either a similar Hopf bifurcation (case A) or a saddle node bifurcation (case B), as in the model with the truncated expansion. Lower panels: Temporal evolution of the total activity $\rho(t)$ on a two-dimensional lattice with $N = 64^2$ (after having introduced noise and coupling); in the (left) synchronous (network spiking) and in the (right) asynchronous (nested oscillations) regimes, respectively, revealing the presence of a synchronization phase transition in between the two regimes; parameter values: $\xi = 5$ and $\xi = 13$, respectively.

Inhibition as main regulatory mechanism. In this section we consider the full Wilson-Cowan equations (1), including both excitatory and inhibitory neural populations for each mesoscopic region or unit. In this case, inhibition plays the role of chief homeostatic mechanism, regulating the level of the overall network activity. More specifically, we consider a version of the Wilson-Cowan

dynamics, including also intrinsic noise as corresponds to large but finite (mesoscopic) regions. Such a model has been recently derived from an underlying microscopic model of spiking neurons in Ref. (3), and is described by the following set of stochastic equations for the densities of excitatory (E) and inhibitory (I) neurons:

$$\begin{aligned}\dot{E}_i &= -\alpha E_i + (1-E_i)\tanh\left[\omega_{EE}E_i - \omega_{IE}I_i + h\right] + \sigma\sqrt{\alpha E_i + (1-E_i)\tanh\left[\omega_{EE}E_i - \omega_{IE}I_i + h\right]} \\ \dot{I}_i &= -\alpha I_i + (1-I_i)\tanh\left[\omega_{EI}E_i - \omega_{II}I_i + h\right] + \sigma\sqrt{\alpha I_i + (1-I_i)\tanh\left[\omega_{EI}E_i - \omega_{II}I_i + h\right]}\,, \end{aligned} \quad [2]$$

where α is the decay rate for the activity, h is an external driving field, σ is the noise amplitude, and ω_{ij} (with $i,j = E,I$) are the couplings between population i and j within a single unit; particularly important here is the auto-excitation coupling ω_{EE}, which we take as a control parameter.

First of all, these equations are analyzed in the (noiseless) mean field limit. By increasing ω_{EE}, the system exhibits a transition from a "down" state to an "up" state (see Fig. 2). Thus, a saddle-node bifurcation separates a state of high activity from a state of low activity, we found no track of a possible Hopf bifurcation. However, as soon as noise is switched on (i.e $\sigma \neq 0$), a noise-induced phenomenon appears: trajectories nearby the up-state fixed point, can escape from its basin of attraction as a result of fluctuations, and are then almost deterministically driven towards the down state, where a similar mechanism makes them escape with some probability. This phenomenon has been recently scrutinized in a remarkable work, where the role of non-normal forms in generating complex dynamics in general and avalanches in particular, has been emphasized (3).

This mechanism, generates in an effective way a noise-induced limit cycle between up and down states, which plays the same role as the deterministic limit cycle (Hopf bifurcation) of case A described in the main text. As a matter of fact, computer simulations of units described by Eq.(2), and coupled diffusively, give rise to the phenomenology illustrated in Fig.2: as the control parameter ω_{EE} is increased, the system undergoes a phase transition from a synchronous phase with very distinctive network spikes, to an asynchronous regime with nested oscillations, as it happens in the model with synaptic plasticity. Thus, also in this case, the phases are the same as in the main text and a synchronization transition appears between them.

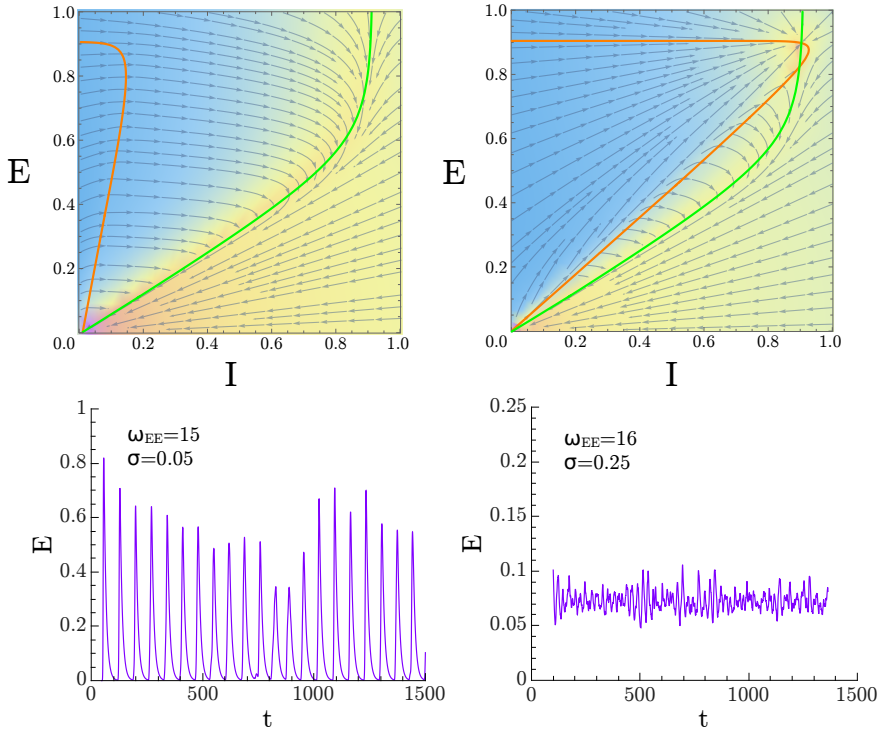

Fig. 2. Upper panels: mean-field analysis of the Wilson-Cowan set of Eqs. (2) describing both excitatory and inhibitory neural populations at each single unit, with parameters such that a noise-induced limit cycle (see (3)) in between a down and an up state can emerge once a non-vanishing noise is switched on. Observe that there is (left) a stable down-state fixed point ($\omega_{EE} = 4$) and a (right) stable up state ($\omega_{EE} = 16$); however the basin of attraction of the up state is small, and a relatively small fluctuation can induce the system state to go beyond the saddle-node line, where deterministic trajectories take the system toward the down state. In the lower panels we illustrate results of a computer simulation for a two-dimensional lattice of coupled noisy units, Eq.(2), corresponding to (left) synchronous/network-spiking and (right) asynchronous/nested-oscillation regimes. Parameter values: $D = 1, \omega_{EI} = 4.65, \omega_{IE} = 14.0, \omega_{II} = 2.8, h = 10^{-3}$ and $\alpha = 0.1$. Control parameter $\omega_{EE} = 15$ for SI regime and $\omega_{EE} = 16$.

SI2. Robustness against changes in synaptic time scales, diffusion and noise. As discussed in the main text, there are two possible scenarios according to the relation between the timescales for the recovery and depletion (τ_R and τ_D, respectively). Namely, between the quiescent or 'down' state with $\rho^* \approx 0$ and the active or 'up' state with self sustained activity there exists a stable limit cycle (case A) or a regime of bistability (case B). Fixing parameter values while changing τ_R and τ_D, it is possible to construct (mean-field or deterministic) a phase diagram showing the different possible cases that emerge when the control parameter ξ is varied (cases A and B). As shown in Fig. 3 when the recovery time (τ_R) is much bigger than the depletion time (τ_D) the system is in the case A, while for bigger values of the depletion time (τ_D) it falls into the case B with a transitions between up (active) and down (quiescent) states.

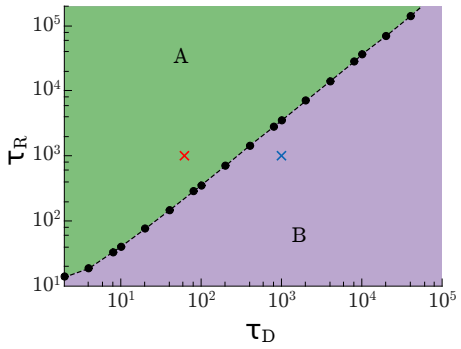

Fig. 3. Mean-field phase diagram showing the type of transition for different values of τ_R and τ_D. Red (blue) cross show the particular case chosen in the Fig.1 of the main text for the case A (B). Parameter values are $a = 0.6, b = 1.3, h = 10^{-3}$.

We have also explored the behavior of the system against changes in the diffusion constant D. Figure 4 shows the phase diagram for different values of D and some particular temporal series with the aim of characterize the different possible behaviors. As can be observed, there exists a transition from the synchronous irregular phase to the synchronous regular one for a wide range of D values (.e.g. from $D = 0.01$ (red line) to $D = 2$ (violet line), and $D = 4$ (green line)). If D is set to very large values, the system falls into the mean field expected behavior, switching from the network spiking regime to the up state. Similar conclusions are obtained, by fixing D and decreasing the noise amplitude σ.

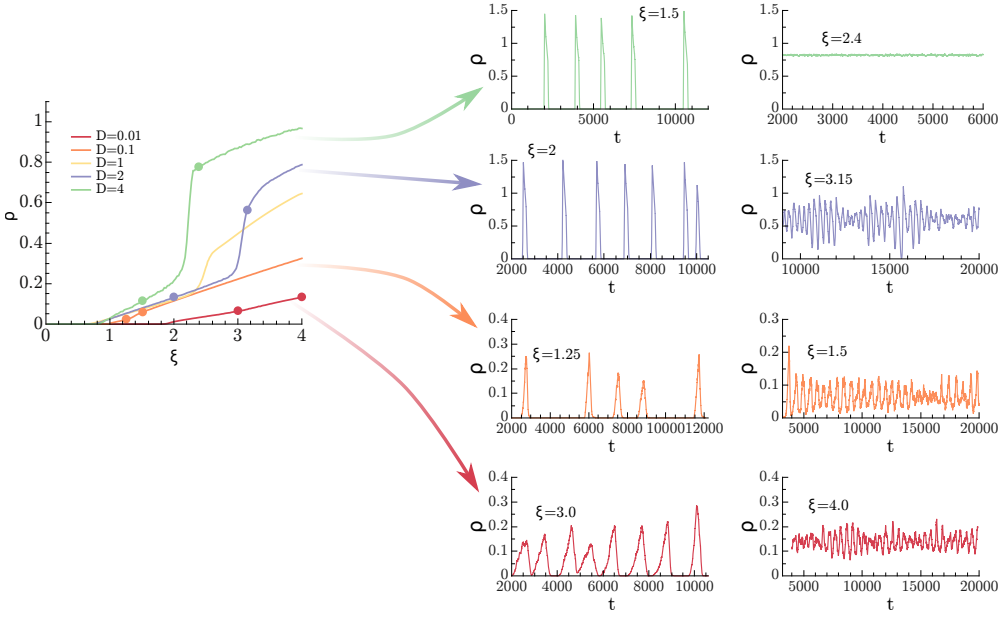

Fig. 4. Left panel: Order parameter as a function of the control parameter ξ for various values of the diffusion constant D. Right panel: Temporal series for two particular values of ξ for each value of D, (marked with colored points in the left panel), showing the expected behavior. Low values of D show a transition between the synchronous irregular phase to the asynchronous irregular one, as in the main text (red, orange, violet and green line). Parameter values: $a = 1.0, b = 1.5, \tau_R = 10^3, \tau_D = 10^2, h = 10^{-7}$.

SI3. The effect of long-range connections and network heterogeneity. The detailed map of synaptic connections plays a central role in brain function (4). Even if most of the neuronal connections occur within the local neighborhood, long-range white-matter connectivity allows for information to be distributed and processed across the whole cortex. Such long-range connections comprise only about 10% of the total connections in the brain, but their role is crucial for brain functionality (4, 5).

Small-world topology. As the simplest possible approximation beyond a lattice of nearest neighbor connections, and consistently with (5), we built a small-world network, as done in the Watts-Strogatz model (6), by rewiring 10% of the links of a two-dimensional lattice. We explored the phase space of the model defined by Eqs. 1 and 2 of the main text, on this connectivity architecture (see Fig.(5) upper panel), and observed that the leading features described in the paper (i.e. phases and phase transitions) are preserved when long-range interactions are introduced. Indeed, as illustrated in the lower part of Fig.(5), our computational analyses reveal that the emergence of synchronous and an asynchronous phase, with a synchronization transition in between is a general intrinsic feature of our model, which is not modified by the small-world property of the network.

In any case, it is important to remark that even if the main phases remain unaffected, important details such as the extension of such phases, the specific shape of avalanches, the amplitude of nested oscillations, the broadness of the critical-like region etc. could be potentially sensitive to the introduction of network heterogeneity. Some of these aspects are explicitly illustrated in the forthcoming paragraphs.

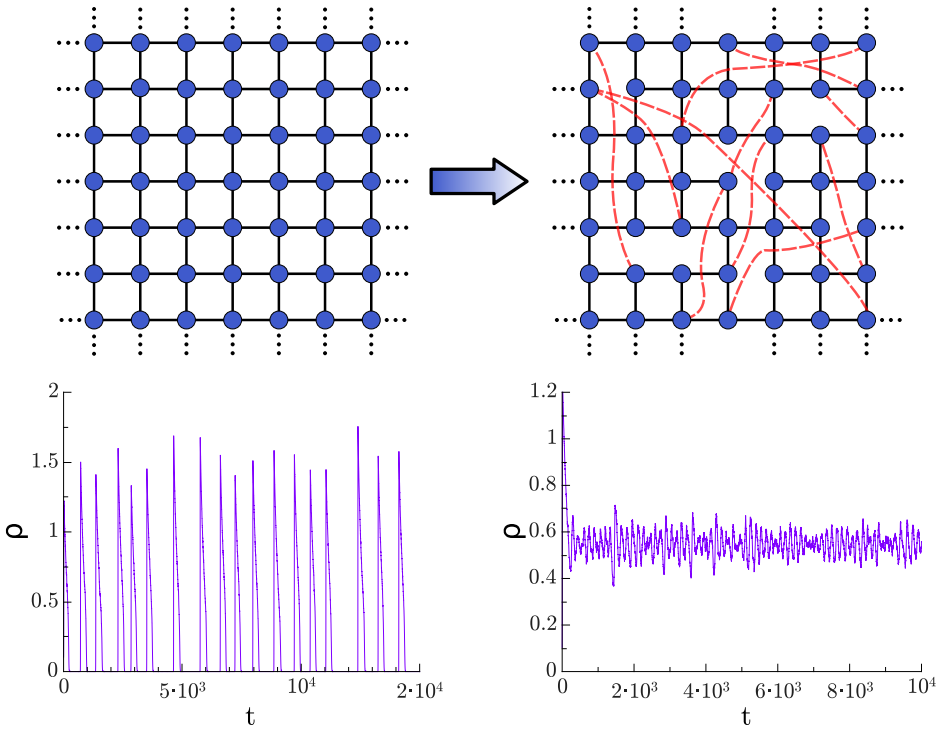

Fig. 5. Upper panel: sketch of the rewiring procedure defining a small-world network architecture: a ten percent of the links are rewired, in such a way that the average connectivity is preserved. Lower panel: Plots illustrating the results of computational analyses of the dynamics (main text, Eq. 1 and 2); in particular, temporal series of the global electrical activity in a small world lattice for two different values of control parameter ξ; (left, $\xi = 2.8$) synchronous/network-spike regime, and (right, $\xi = 2.96$) asynchronous/nested-oscillation regimes, respectively; a synchronization phase transition exists separating these two alternative regimes. Other parameter values: $a = 1.0, b = 1.5, \tau_D = 10^2, \tau_R = 10^3, h = 10^{-7}$.

Clustered and heterogeneous networks. Recent experimental analyses have scrutinized the effect of network heterogeneity in cultures of rat cortical neurons *in vitro* (7). In particular, Okujeni *et al.* where able to control the level of clustering by experimentally modifying the level of a given enzyme (protein Kinase C) that promotes neuronal aggregation. In this way, progressively more clustered networks were generated as the level of protein was increased (see Fig. 1 in (7)).

Keeping fixed other experimental conditions, Okujeni *et al.* found that in the case in which neurons are more homogeneously distributed in the substrate networks spikes appear much more sporadically than when the network is highly clustered (see Fig. 7, which is adapted from (7)), and that network spikes appear more clustered in time in this latter case. Thus, in conclusion, clustering promotes the generation of spontaneous network activity.

In order to model these experimental results, we developed a heterogeneous network in which we keep fixed the mean value of the parameter a (that controls the decay of the activity at each single unit), but inducing some areas with low local values of a_1, i.e. with a smaller propensity for activity to decay (red nodes in Fig. 6), while in the rest of the network larger values of a, a_2, are considered (keeping the network-average value of a constant).

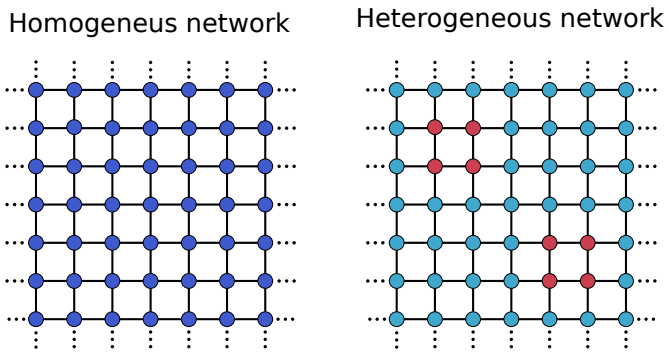

Fig. 6. Sketch of the considered networks: homogeneous to the left and heterogeneous/clustered to the right. In both cases the network-average value of the activity-decay parameter a is taken to be equal. However, while in the homogeneous case the value of a is constant across the network, in the heterogeneous one there are some areas (marked with red nodes) with a lower value of a.

As shown in Figure 7, the lower the local value of a_1, the more facilitated the emergence of spontaneous activity, leading the system closer and closer to the critical point or the asynchronous irregular phase, and reproducing quite remarkably the chief experimental observations of Okujeni *et al.*

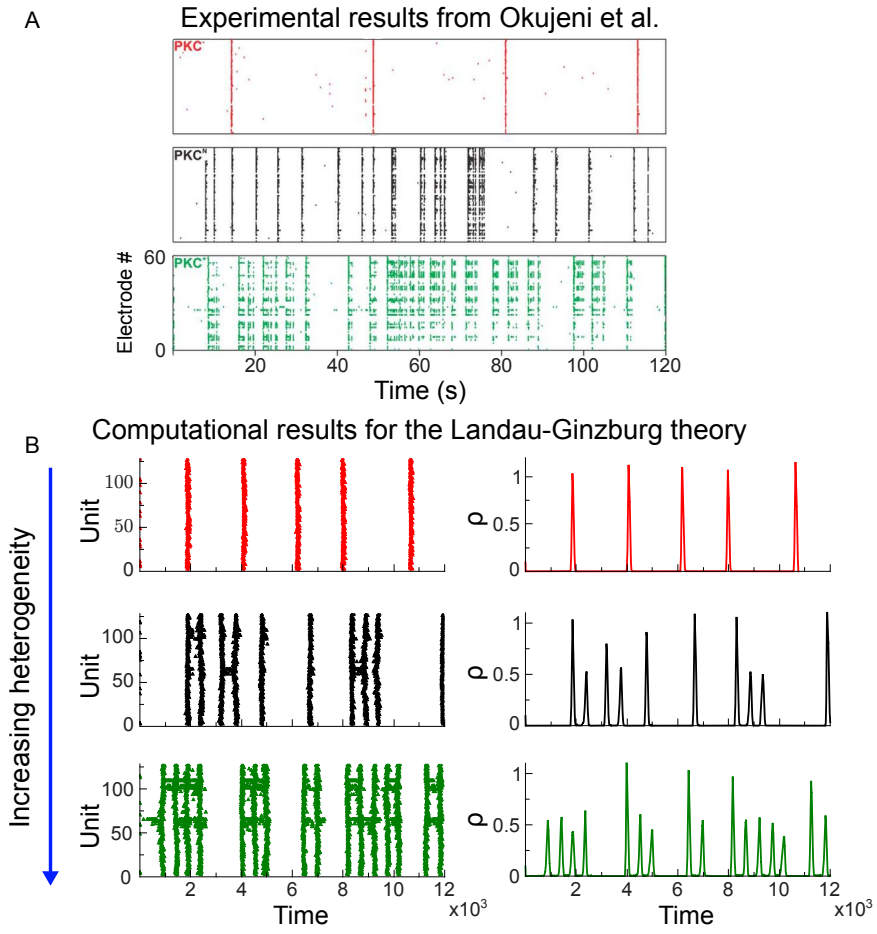

Fig. 7. Temporal series for different level of network clustering. Panel A shows the experimental results of Okujeni (7) (adapted figure from the original paper) for increasing levels of aggregation in a neural network. Panel B shows three temporal series for different levels of network clustering and a fixed value of $\xi = 1.2$. In the first one (red) the network is homogeneous with $a_1 = a_2 = 1$. Observe that smaller values of a_1 produce a more active network, in particular for $a_1 = -0.7$ (black) and $a_1 = -0.928$ (green). In both cases, the clustering facilitate the spontaneous activity. Other parameter values: $b = 1.5, \tau_D = 10^2, \tau_R = 10^3, h = 10^{-7}$.

Thus, in conclusion, our general model, equipped with an additional layer of network heterogeneity is able to reproduce specific empirical results.

SI4. Detrended Fluctuation Analysis. In this section we present an additional type of analyses to discriminate whether the system lays at a critical point or in either the subcritical or the supercritical phases. The method is based on the fact that, at the critical point of a continuous phase transition, the (time-dependent) order parameter, as measured in any finite system, shows long-range temporal correlations (i.e. long-memory effects), which can be quantified by measuring its Hurst exponent (8). The Hurst exponent of a time series is a measure of the dispersion of a process on a scaling support. For example the Hurst exponent of an uncorrelated signal (white noise) is $\alpha = 1/2$, since the root mean square translation distance after n steps of a Wiener process, i.e. an unbiased random walk (the process obtained by integrating white noise), is proportional to $\sqrt{n}$. For correlated signals (colored noises) one expects bigger Hurst exponents (as a reference, $\alpha \simeq 1$ is found for pink noise). The Hurst exponent can be calculated by splitting the time series into adjacent windows, plotting the square-root displacement from the mean as a function of the window size and evaluating the exponent of the resulting power law (see below). More specifically, "detrended fluctuation analysis" (DFA) is a technique for measuring the Hurst exponent in non-stationary time series: the "detrending" operation allows to remove fictitious memory effects related to non-stationarity, and the method basically consists in subtracting the local "trend" (usually using a linear fit approximation) of the signal before performing the analysis on each window (9, 10). DFA consists of two steps: the data series $\rho(t)$ is shifted by its mean $\bar{\rho}$, and integrated (cumulatively summed) in time:

$$\mathcal{P}(\tau) = \sum_{t=1}^{\tau} (\rho(t) - \bar{\rho}) \,; \qquad [3]$$

then segmented into k windows of various sizes n, and for each window size, a fluctuation function $F(n)$ is calculated, as

$$F(n) = \sqrt{\frac{1}{T} \sum_{h=1}^{k} \sum_{\tau=1}^{n} \left(\mathcal{P}^{(n)}(\tau + (h-1)n) - X_{\mathcal{P}}^{(n)} \right)^2} \qquad [4]$$

where $X_{\mathcal{P}}^{(n,h)}$ is the linear regression of $\mathcal{P}^{(n)}(\tau)$, with $\tau \in [(h-1)n, hn]$, the superscript indicates the dependence on the window size n and $T = kn$ is the total length of the time series. If $F(n) \sim n^{-\alpha}$, then α is the Hurst exponent (9, 11).

We performed a DFA on the global signal $\rho(t)$ coming out of our computer simulations for different values of the control parameter ξ (in the synchronous and asynchronous phases as well as at the critical point). Results are shown in Fig.8: (i) fluctuations in the asynchronous phase grow approximately as the square root of the window length, as expected for (uncorrelated) white noise; (ii) in the synchronous phase, above a certain characteristic length, the dependence is very weak, remarking the existence of a certain degree of order, i.e. a characteristic time scale at which there is order, i.e. synchronization; (iii) just at the critical point the growth of the fluctuations is anomalously large, confirming the existence of long-range correlations: a signature of criticality. Therefore, from the global activity signal we are able –through a DFA analysis– to conclude that long-range correlations, characteristic of criticality, emerge at the transition point.

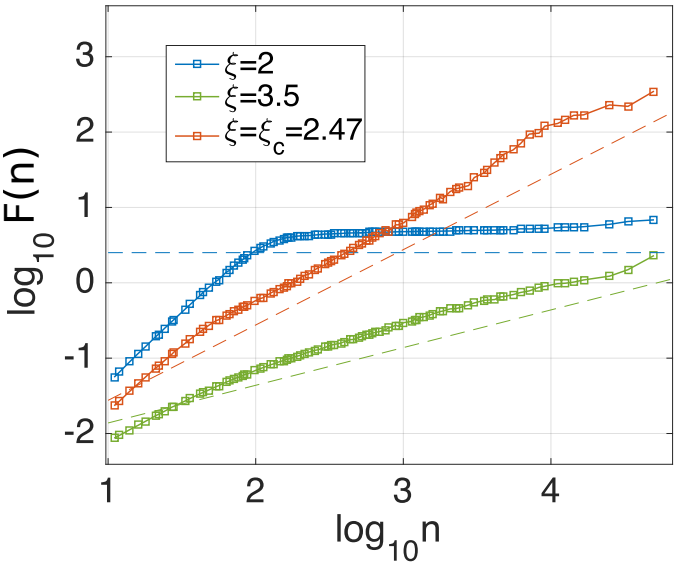

Fig. 8. Detrended fluctuation analysis of the macroscopic signal for different values of the control parameter $\xi = 2$ (synchronous phase) $\xi = 2.47$ (critical point), and 3.5 (asynchronous phase), respectively. Close to the transition point the DFA shows an Hurst exponent close to 1 (orange dashed line) implying long-range autocorrelations, a fingerprint of criticality, while the white noise value $\alpha = 1/2$ (green dashed line) emerges in the asynchronous regime, and an asymptotically almost flat curve is obtained in the synchronous phase, revealing the existence of a characteristic time scale. Parameter values are taken as in the main text and $N = 2^{14}$.

SI5. The nature of nested oscillations. In order to unveil the nature of the nested oscillation (asynchronous irregular, (AI)) phase and to determine whether it is a finite size effect or it survives in the thermodynamic limit, the existence of a second phase transition separating it from the up state is investigated here. In other words: are the asynchronous irregular phase and the up-state phase two different phases, or are they just the same phase, with only a quantitative difference in the amplitude of the variability around the mean value? As we illustrate in what follows the correct answer is this second one.

In principle, these two regimes show a qualitative difference: in the AI phase each single unit keeps switching between the *on/up* and *off* states and there exists a macroscopic fraction of *off/down* sites, whereas in the active phase units are permanently in the *on* state and, even if fluctuations might lead some unit to the *off* state, the macroscopic fraction of them vanishes (see Supplementary Movie). The fraction of inactive units, ρ_0, can thus be chosen as an order parameter for the putative phase transition between the AI and the active phase. In Figure 9 we plot the average over time of ρ_0 in function of ξ and we verify that this alternative order parameter detects the same phase transition already characterized in the main text, by employing synchronization order parameters. This implies that, in the large system-size limit, there exists no macroscopic difference between the asynchronous/nested-oscillation regime and the up state. Therefore, the nested oscillations can be understood as the result of partial synchronization of local regions; the superposition of a few regions gives rise to complex waves as those in Fig.2 (A3) of the main text. However, when the system becomes progressively large, the number of such locally synchronized regions grows, and their interference leads to a standard up state, in which fluctuations around the mean density decay as a function of the system size.

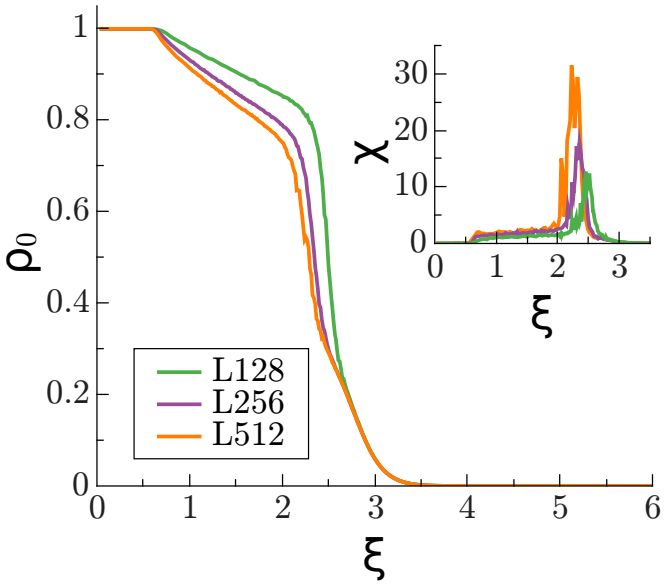

Fig. 9. Main: averaged fraction of inactive sites in the system ρ_0 as a function of the control parameter ξ, revealing the presence of a phase transition. Inset: Variance over runs of a given fixed duration of the average value of the control parameter multiplied by $\sqrt{N}$ in order to highlight possible deviations with respect to central limit theorem (CLT); as a result of which, a decay with $\sqrt{N}$ is expected; thus multiplying by $\sqrt{N}$ a convergence to a constant should be expected if the CLT holds. Observe, however, the increase in peak height as the system size is enlarged revealing a violation of the CLT, as expected at the critical point of a second order phase transition. Note that for all the system sizes the peaks are located approximately in the same spots as in Fig.4 in the main text; thus ρ_0 is an alternative order parameter that leads to the same results as the previously considered synchronization order parameters: it detects the synchronization phase transition, and reveals that there is no difference between the AI and the active phase in the limit of infinitely-large network sizes.

SI6. Definition and analyses of avalanches.

On the definition of spiking events. In the analysis of avalanches presented in the main text, a particular (and reasonable) criterion has been chosen to convert each local (continuous) time signal into a discrete series of spikes, allowing to build up the raster plot, from which avalanches are measured using the standard experimental protocol consisting on a time-clustering the events (12).

Here, we employ a different criterion to define spikes, thereby illustrating the robustness of our main findings against such a choice. In particular, the alternative discretization criterion is sketched in Figure 10 and is as follows: a threshold θ is established at each single unit, and every unit is declared to be in its *spiking* (or "on") state whenever its activity is over threshold. Thus, the main difference with the protocol in the main text is that now, in between two-consecutive time steps in which the unit is below threshold, the site is considered to be "on" not just at one time step (at its maximum of activity, as in the method of the main text), but possibly during many time steps, in a full time interval.

Considering these spiking events, avalanches are defined through the same experimentally inspired protocol that we used in the main text; the size of an avalanche is simply the number of spike counts during an avalanche. Figure 10 shows that the avalanche size distribution at the critical point is preserved by employing this alternative definition of the spikes. Moreover if a (random) subsampling of the units is performed, the distribution keeps following a power law which is roughly consistent with the experimentally measured exponent $3/2$.

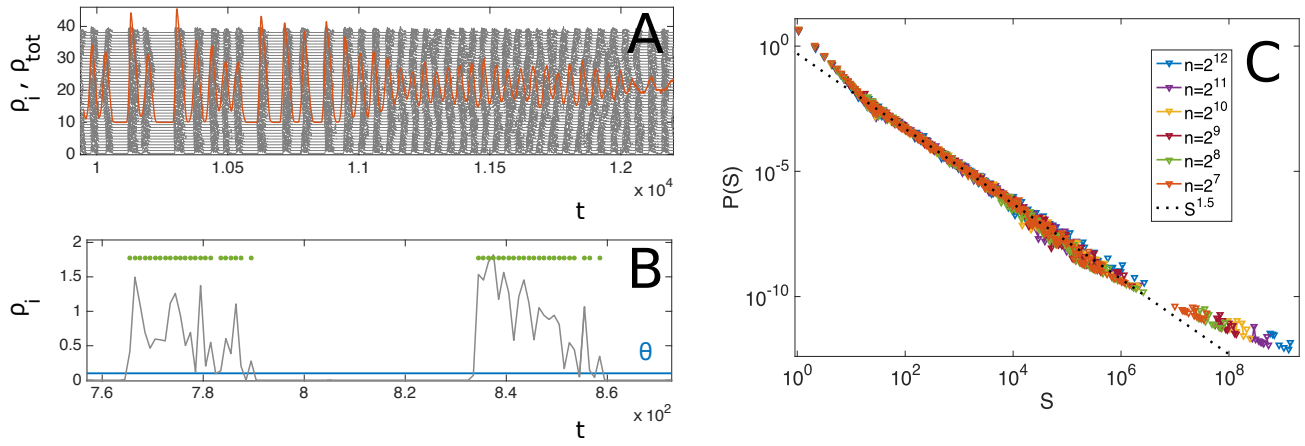

Fig. 10. A. Sample of local temporal signals are plotted in grey (shifted for convenience of visualization) together with the global signal $\rho(t)$ (shifted and rescaled) represented in red color, for a lattice of $N = 64^2$ units. B. illustration of the alternative method employed here to define "spike events" from a local temporal signal. Green dots represent times during which the unit is in its spiking state; obviously, a discrete (integration) time is required to have a finite number of spikes per interval of local activity. C. Distribution of avalanche sizes for various subsampling trials, using the criterion sketched in B to define events. The black dotted line is the power law with exponent $3/2$ plotted as a guide to the eye.

Threshold effects. The standard empirical method to detect avalanches, as defined in (12), is intrinsically affected by some arbitrariness in parameter choices, that has been already discussed in the literature (12, 13). In particular, one arbitrary parameter is the threshold value θ above which the state "on" or "spiking" is declared [*] The common belief is that if, as a matter of fact, the system is scale-invariant, this value should not affect the large scale properties, such as exponent values. However, one has to be particularly careful with any thresholding procedure. For example, while for a standard one-dimensional random-walk process the avalanche exponents are independent of the threshold value chosen, this is not the case for other stochastic processes, e.g. birth-death processes (14). Moreover the threshold value should not be chosen too high relatively to the amplitude of the signal in order to avoid splitting an event into multiple (correlated) ones (15).

Recording a spike every time that the system crosses a very small threshold exposes the measurements to the effects of small fluctuations around the origin, induced by the multiplicative demographic noise term in Eq.1 in the main text (see Fig. 11). In order to avoid such a problem, it is possible to set also a second threshold value A_{min} for the minimal area for a spiking event to be considered as such; below such a threshold, activity is considered just a noise effect and, hence, disregarded. As illustrated in Figure 12 the statistics of avalanches does not depend significantly on the value chosen for such a threshold, A_{min}.

[*] In order to avoid spurious effects and consistently with the definition of avalanches as activity propagating marginally before falling into an absorbing state ($\rho = 0$), we choose a small value $\theta \ll 1$ (namely $\theta = 10^{-4}$).

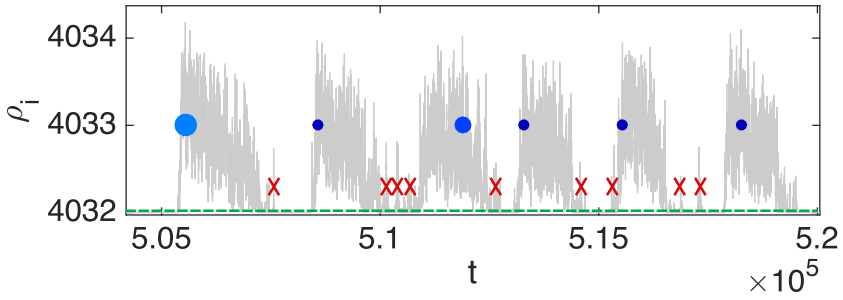

Fig. 11. Illustration of small events in the signal of the activity of one unit. Events covering a very small area (marked with red crosses) are neglected, while proper spikes are marked with blue full dots (smaller darker dots correspond to spikes with smaller area).

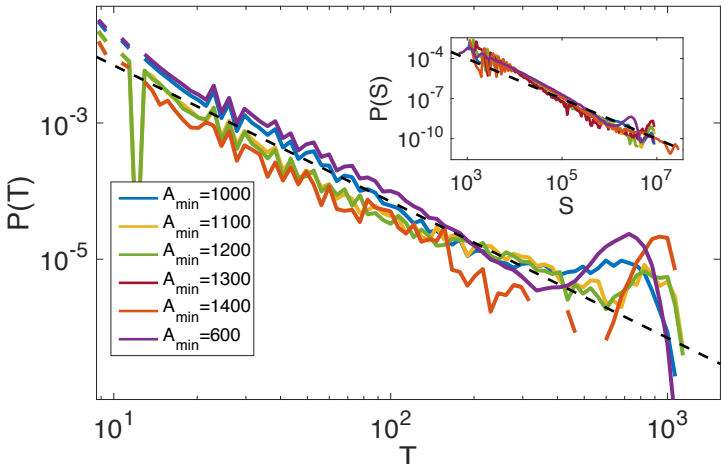

Fig. 12. Independence on the avalanche exponent values on the value chosen for the threshold on the minimal area A_{min}, used to declare "activity". Apart from the details of the substructure of the distribution, no qualitative dependence can be found by varying the value of A_{min}, both in avalanche-time (main plot) and avalanche-size (inset) distributions.

Experimentally inspired procedure to measure avalanches. Here, we briefly explain the steps necessary to perform a measure of an avalanche's size and duration, starting from a raster plot, as usually done in experimental setups (12). First of all, the Inter-Spike-Interval (ISI) is measured, as the average time interval between two consecutive spikes of (whichever 2 elements of) the network. Then the raster plot is divided in contiguous bins of width equal to the IEI (see Fig.5C in the main text). A bin is considered "empty" if no events are reported within it, and "occupied" otherwise. Consecutive series of occupied bins, preceded and ended by an empty one, define an avalanche. The avalanche duration is just the time interval between the preceding and the ending empty bins, and avalanche size is the total number of spikes that occurred in that time-interval. Since the individual signal in our analysis stems from a coarse grained section of neural tissue, we assign a weight to each event, representing the number of spikes within it, and determined by the integral of the signal during the event (see Fig.5A). Thus the only difference between the procedure we employ and the experimental one (12) is that the size of an avalanche is defined in our case as the *weighted* sum of the events during an avalanche.

System-size dependence. At the critical point of a phase transition, scale-invariant behavior is expected to be only limited by system size. This effect, which has been reported to be observed in experiments on neural avalanches (12), is also a hint in favor of true scale invariance, since finite size scaling holds when the system is at its critical point. In Figure 13 avalanche size and duration distributions are compared for various system sizes; as expected, larger systems show larger avalanches with progressively larger cut-off scales, while the overall size (resp. time) distribution keeps following a power law trend with the usual exponents $\tau = 3/2$ (resp. $\alpha = 2$; see inset).

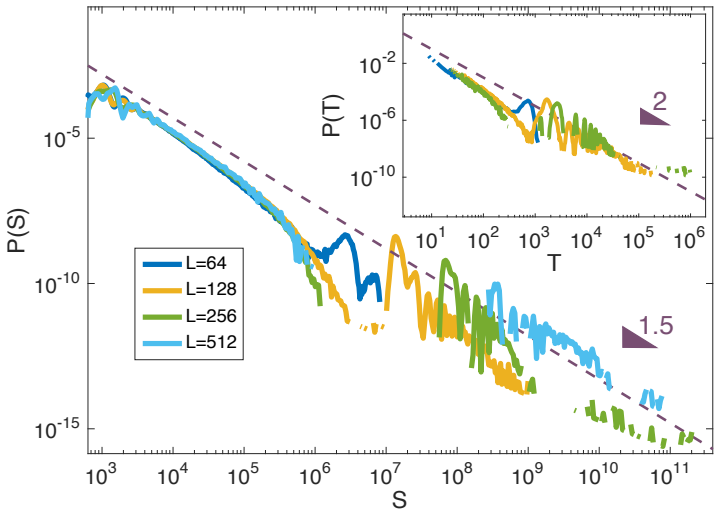

Fig. 13. Avalanche size S and duration T distributions for system sizes $N = 2^{12}, 2^{14}, 2^{16}, 2^{18}$. Although finite size scaling is not perfect, as the system size grows progressively larger, larger avalanches are found. Dashed lines represent an hypothetic power law trend with $\tau = 3/2$ and $\alpha = 2$.

SI7. Oscillations coexisting with scale invariance. Usually, scale-free avalanches of activity can be measured at the critical point of an *absorbing-state phase transition*. When the concept of "avalanche" is employed to describe the critical point of a synchronization phase transition, the marginal oscillatory nature of the system introduces a characteristic time scale in the synchronous phase –i.e. the period of the oscillations– which, in principle, is in contrast with the idea of scale-invariance. However, the two concepts can coexist –at least within certain limited scales– as illustrated in Figure 14. It shows that the structure (e.g. the peaks) in the avalanche-time distribution (inset) corresponds to the period of oscillation of a macroscopic variable (the total number of spikes, in the main plot); for instance, an isolated network synchronization event has a typical duration of 2000 (in arbitrary units), a sequence of two, about 5000, etc. On the other hand, the whole distribution, once these peaks are ignored can be approximately described as a power law with the expected exponent value.

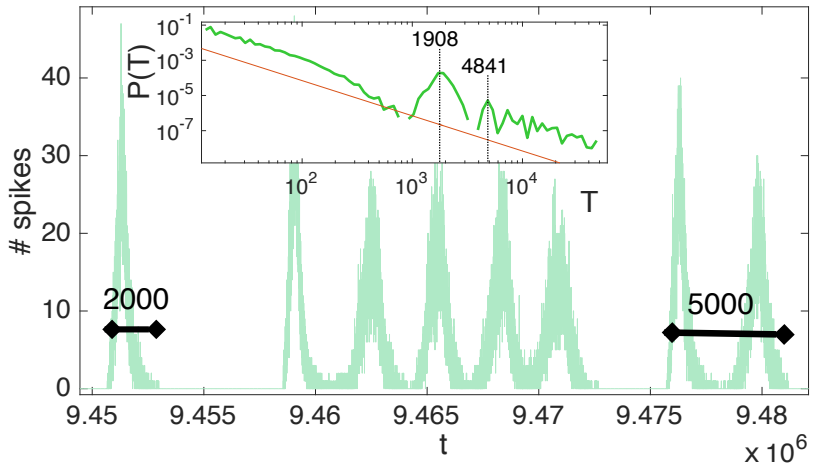

Fig. 14. Analysis of the structure underlying the avalanche-duration distributions. The main figure shows the total number of spikes at time t. Irregular oscillations of the global activity can be recognized, as the system is close to the edge of the synchronization phase transition. The characteristic period of an isolated oscillation corresponds to the peak in the avalanche duration distribution, while its multiples correspond to smaller peaks. System size $N = 128^2$.

REFERENCES

1. Wilson HR, Cowan JD (1972) Excitatory and inhibitory interactions in localized populations of model neurons. *Biophys. J.* 12(1):1–24.
2. Markram H, Tsodyks M (1996) Redistribution of synaptic efficacy between pyramidal neurons. *Nature* 382:807–810.
3. Benayoun M, Cowan JD, van Drongelen W, Wallace E (2010) Avalanches in a stochastic model of spiking neurons. *PLoS Comput. Biol.* 6(7):e1000846.
4. Sporns O (2010) *Networks of the Brain.* (MIT Press, USA).
5. Jbabdi S, Sotiropoulos SN, Haber SN, Van Essen DC, Behrens TE (2015) Measuring macroscopic brain connections in vivo. *Nat Neurosci* 18(11):1546–1555.
6. Watts DJ, Strogatz SH (1998) Collective dynamics of small-world networks. *Nature* 393(6684):440–442.
7. Okujeni S, Kandler S, Egert U (2017) Mesoscale architecture shapes initiation and richness of spontaneous network activity. *J. Neurosci.* 37(14):3972–3987.
8. Mantegna RN, Stanley HE (1999) *Introduction to econophysics: correlations and complexity in finance.* (Cambridge university press).
9. Peng C, Havlin S, Stanley HE, Goldberger AL (1995) Quantification of scaling exponents and crossover phenomena in nonstationary heartbeat time series. *Chaos: An Interdisciplinary Journal of Nonlinear Science* 5(1):82–87.
10. Hu K, Ivanov PC, Chen Z, Carpena P, Stanley HE (2001) Effect of trends on detrended fluctuation analysis. *Phys. Rev. E* 64(1):011114.
11. Linkenkaer-Hansen K, Nikouline VV, Palva JM, Ilmoniemi RJ (2001) Long-range temporal correlations and scaling behavior in human brain oscillations. *Journal of Neuroscience* 21(4):1370–1377.
12. Beggs JM, Plenz D (2003) Neuronal avalanches in neocortical circuits. *J. of Neurosci.* 23(35):11167–11177.
13. Petermann T, et al. (2009) Spontaneous cortical activity in awake monkeys composed of neuronal avalanches. *Proc. Natl. Acad. Sci. USA* 106(37):15921–15926.
14. Font-Clos F, Pruessner G, Moloney NR, Deluca A (2015) The perils of thresholding. *New J. Phys.* 17(4):043066.
15. Laurson L, Illa X, Alava MJ (2009) The effect of thresholding on temporal avalanche statistics. *J. Stat. Mech. Theory E* 2009(01):P01019.